Supporting Information

Engineered pH-Responsive Mesoporous Carbon Nanoparticles for Drug Delivery

Miguel Gisbert-Garzarán,[1,2‡] Julia C. Berkmann,[3,4‡] Dimitra Giasafaki,[5] Daniel Lozano,[1,2] Konstantinos Spyrou,[6] Miguel Manzano,[1,2] Theodore Steriotis,[5] Georg N. Duda,[3,4,7] Katharina Schmidt-Bleek,[3,4] Georgia Charalambopoulou,[5]* and María Vallet-Regí[1,2]**

[1]Department of Chemistry in Pharmaceutical Sciences, Faculty of Pharmacy, Universidad Complutense de Madrid, Instituto de Investigación Sanitaria Hospital 12 de Octubre (imas12), Plaza Ramón y Cajal s/n, 28040 Madrid, Spain.

[2]Networking Research Center on Bioengineering, Biomaterials and Nanomedicine (CIBER-BBN), Madrid, Spain.

[3]Julius Wolff Institute and Center for Musculoskeletal Surgery, Charité—Universitätsmedizin Berlin, Berlin, Germany.

[4]Berlin-Brandenburg School for Regenerative Therapies, Charité —

Universitätsmedizin Berlin, Berlin, Germany.

[5]National Center for Scientific Research "Demokritos", 15341 Agia Paraskevi

Attikis, Athens, Greece.

[6]Department of Materials Science and Engineering, University of Ioannina, GR-

45110 Ioannina, Greece.

[7]Berlin Institute of Health Center for Regenerative Therapies, Berlin, Germany.

‡ Both authors contributed equally to this work.

*Corresponding authors.

E-mail: Katharina.Schmidt-Bleek@charite.de

E-mail: gchar@ipta.demokritos.gr

E-mail: vallet@ucm.es

Analytical methods

Small Angle X-ray Scattering (**SAXS**) measurements were carried out in transmission mode on a Rigaku SmartLab X-ray diffraction system equipped with SAXS optics (λ=1.54 Å). The scans were obtained from 0.06 to 8 degrees with a step of 0.02 degrees and a speed of 0.1 deg/min. Scanning Electron Microscopy (**SEM**) analysis was performed using a JEOL JSM 7401F Field Emission Microscope equipped with Gentle Beam mode. A low acceleration voltage was applied (~ 2kV), and the working distance was set to 3 mm. The samples, in the form of a fine powder, were mounted onto a round brass substrate using double-coated conductive carbon tape. Magnification: C3: x10000 (inset: x30000); C1Sph: 30000. Transmission Electron Microscopy (**TEM**) images were recorded on a JEOL JEM 2100 (Electron Microscopy Centre, UCM). Sample preparation was performed by dispersing the materials in distilled water and subsequent deposition onto carbon-coated copper grids. **Nitrogen adsorption/desorption** (77 K) and **Helium pycnometry** (300 K) **measurements** were carried out on a volumetric gas adsorption analyzer (Autosorb-1-MP, Quantachrome), using ultra-pure N_2 (99.999 %) and helium (99.999%). Prior to measurement, samples were appropriately outgassed under high vacuum (10^{-6} mbar). The BET area values were calculated following the BET consistency criteria (ISO 9277:2010), while pore size distributions were deduced by using the N_2-carbon QSDFT (Quenched Solid Density Functional Theory) kernel for slit-cylindrical pores (adsorption

model). Micropore volumes were assumed to be the QSDFT derived cumulative volumes for pores smaller than 2 nm. The total (micro and meso) pore volumes (TPV) were estimated from the amount adsorbed at p/p_0 = 0.95 (C3) or 0.90 (C1Sph) in order to avoid contributions from the external surface and/or large pores. X-ray photoelectron spectroscopy (**XPS**) measurements for the plain and the polymer-coated carbons were performed under ultrahigh vacuum conditions with a base pressure of 3.8 x 10^{-10} mbar in a SPECS GmbH instrument equipped with a monochromatic MgKa source (hv = 1253.6 eV) and a Phoibos-100 hemispherical analyzer. Pulverized samples were dispersed in water, and after short sonication and stirring, a minute quantity of the suspensions was drop casted on silicon wafers and left to dry in air before transferring to ultrahigh vacuum. The energy resolution was set to 1.2 eV and the photoelectron take-off angle was 45° with respect to the surface normal. Recorded spectra were the average of 4 scans with energy step set to 0.05 eV and dwell time 1 s. All binding energies were referenced to the C1s core level at 284.8 eV. Spectral analysis included a Shirley background subtraction and peak deconvolution employing mixed Gaussian-Lorentzian functions, in a least squares curve-fitting program (WinSpec) developed at the Laboratoire Interdisciplinaire de Spectroscopie Electronique, University of Namur, Belgium.

Nuclear Magnetic Resonance (**NMR**) spectroscopy was carried out on a Bruker AV250 MHz. Thermogravimetric (**TGA**) measurements were performed on a Perkin Elmer Pyris Diamond TG/DTA analyzer by placing 10 mg of sample

in an aluminium crucible and applying 5°C/min heating ramps from room temperature (RT) to 600°C. **Fluorescence spectrometry** was carried out in a BioTek Spectrofluorimeter. Dynamic Light Scattering (**DLS**) measurements were carried out on a Zetasizer Nano ZS (Malvern Instruments Ltd.) after dispersing the samples in water.

Additional characterization

ORGANIC COMPOUNDS

The synthetic path for the synthesis of self-immolative polymers is depicted in Scheme **S1**.
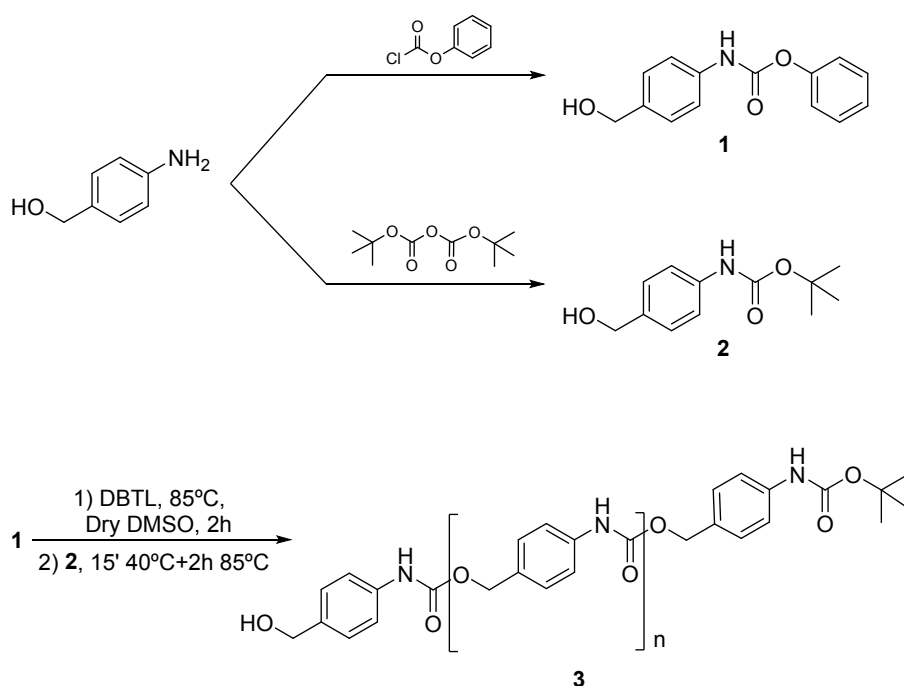
Scheme S1. Synthetic path of monomer (**1**), trigger (**2**) and self-immolative polymer (**3**).

The above-mentioned compounds were characterized in terms of ^{1}H-NMR, where the obtained signals indicate the successful synthesis (Figures **S1** to **S3**).
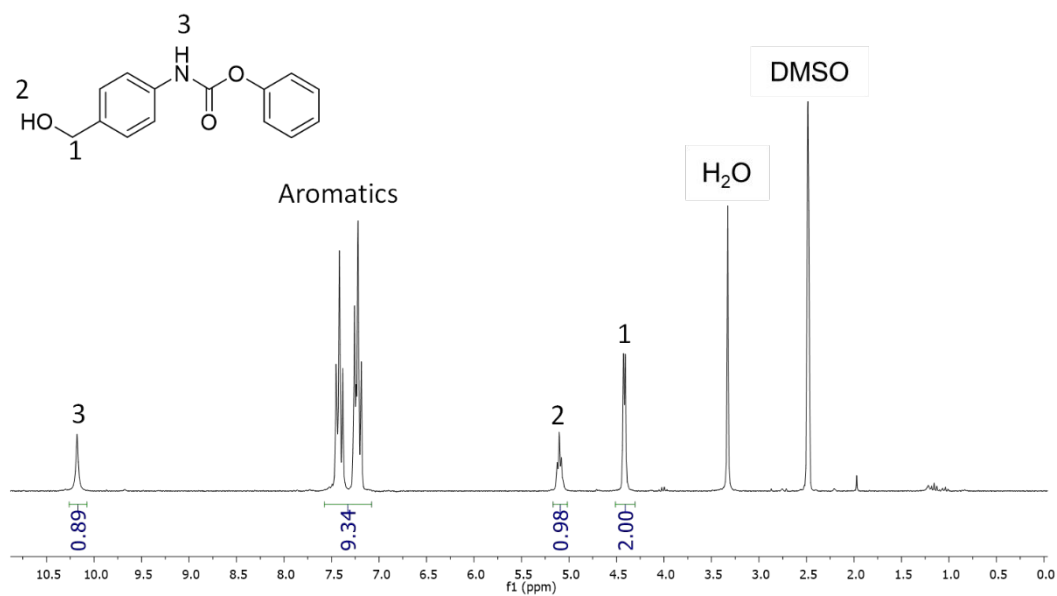

Figure S1. ^{1}H NMR of compound 1. 1H NMR (250 MHz, DMSO) δ 10.20 (s, 1H), 7.25-7,45 (m, 9H), 5.12 (t, 1H), 4.45 (d, 2H).
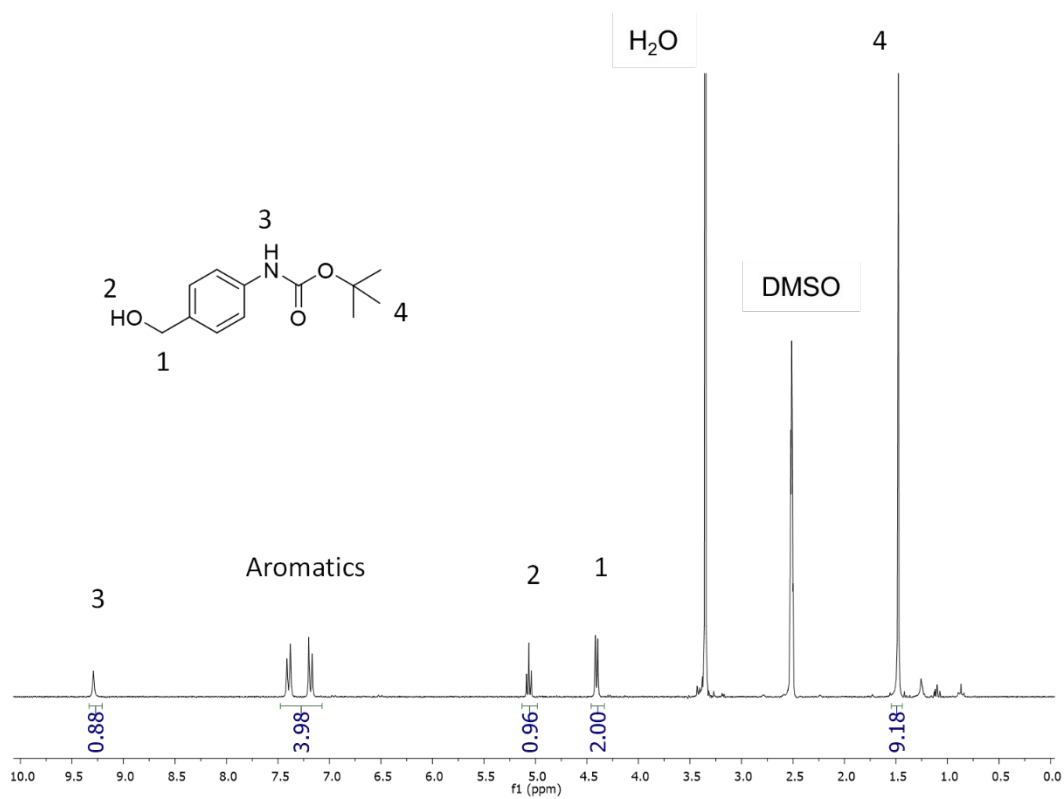
Figure S2. ^{1}H NMR of compound 2. 1H NMR (250 MHz, DMSO) δ 9,29 (s, 1H), 7.17-7,41 (m, 4H), 5.05 (t, 1H), 4.40 (d, 2H), 1,48 (s, 9H).
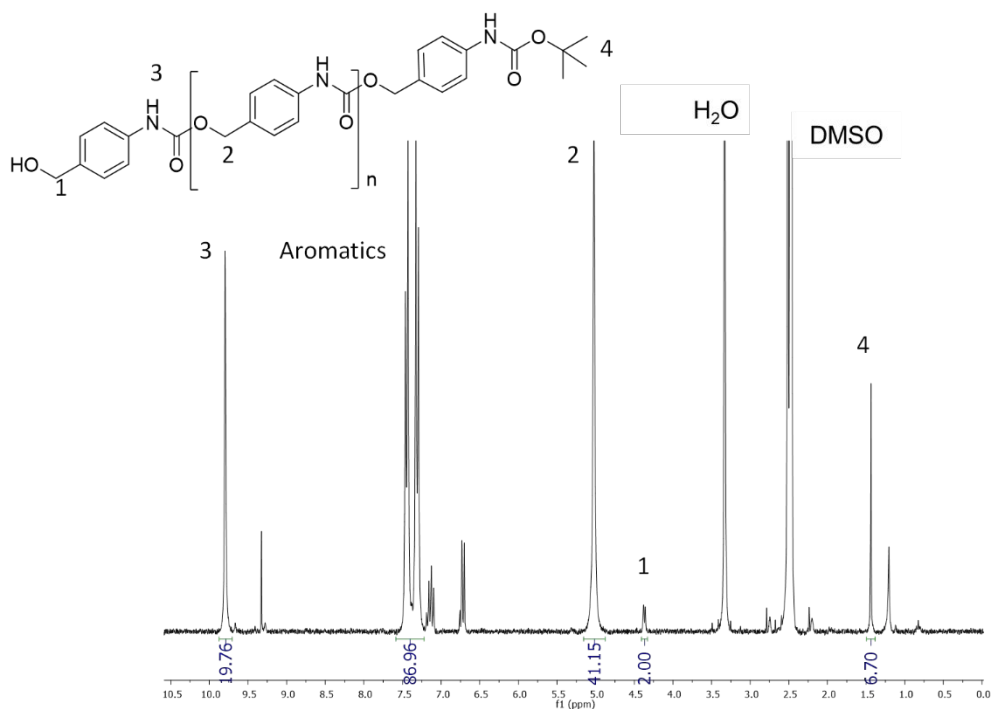
Figure S3. ^{1}H NMR of compound 3. 1H NMR (250 MHz, DMSO) δ 9.82 (s, 19H), 7.56-7.15 (m, 96H), 5.15(s, 41H), 4.43 (d, 2H), 1.48 (s, 9H).

The number of units of each chain was calculated from the ratio benzylic hydrogens at the molecule tail *vs.* those in the polymeric carbon. In this case, the polymer would have 20 units. Signal 4 indicates the pH-responsive trigger.

PRISTINE AND HYBRID CARBON MATERIALS
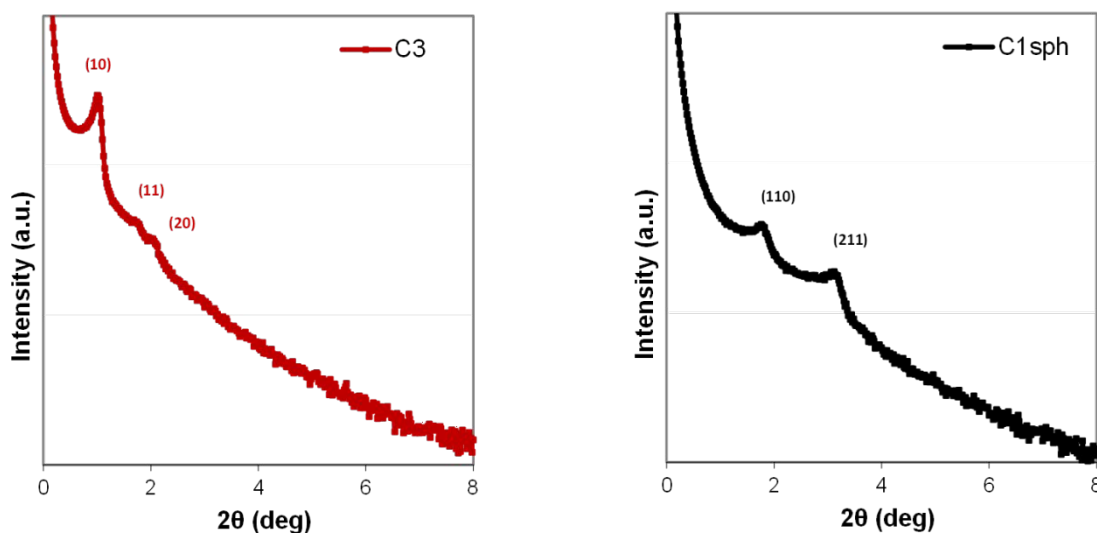
SAXS measurements of C3 and C1Sph.

Figure S4: SAXS of C3 (left) and C1Sph (right). In both cases the diffraction peaks are characteristic of the expected pore symmetry.

N$_2$ adsorption-desorption measurements of C3 and C1Sph

The porosity of the carbon materials was analyzed by N$_2$ adsorption–desorption measurements at 77 K. The obtained isotherms, along with the corresponding pore size distributions, are presented in Figure S5. The nitrogen adsorption isotherm of the C3 material corresponds to a type IV material (based on IUPAC classification) with H2(a) hysteresis loop, typical of CMK-3 type mesoporous materials, with uniform small mesopores of *ca.* 4.5 nm and additional microporosity.[1–3] The isotherm of the C1Sph material, apart from a minute H4 hysteresis loop, exhibits a stepwise behavior indicative of the CMK-1 type mesoporous materials with high degree of uniformity of narrow mesopores of *ca.* 3.2 nm in size, as well as a significant amount of micropores.[1–3] The increase of the N$_2$ uptake for p/p$_0$ > 0.90 for both samples points to the presence of external

surface area and/or macroporosity formed by the interparticle voids. In the case of C3 this increment is not significant, while in the case of C1Sph the agglomeration of the carbon spheres leads to a considerable secondary large meso-to-macro-pore volume (V = 1.8 cm^3 g^{-1} based on amount adsorbed at p/p_0 = 0.99, pore diameter ~40-60 nm) providing thus significant additional volume for sorption of APIs.
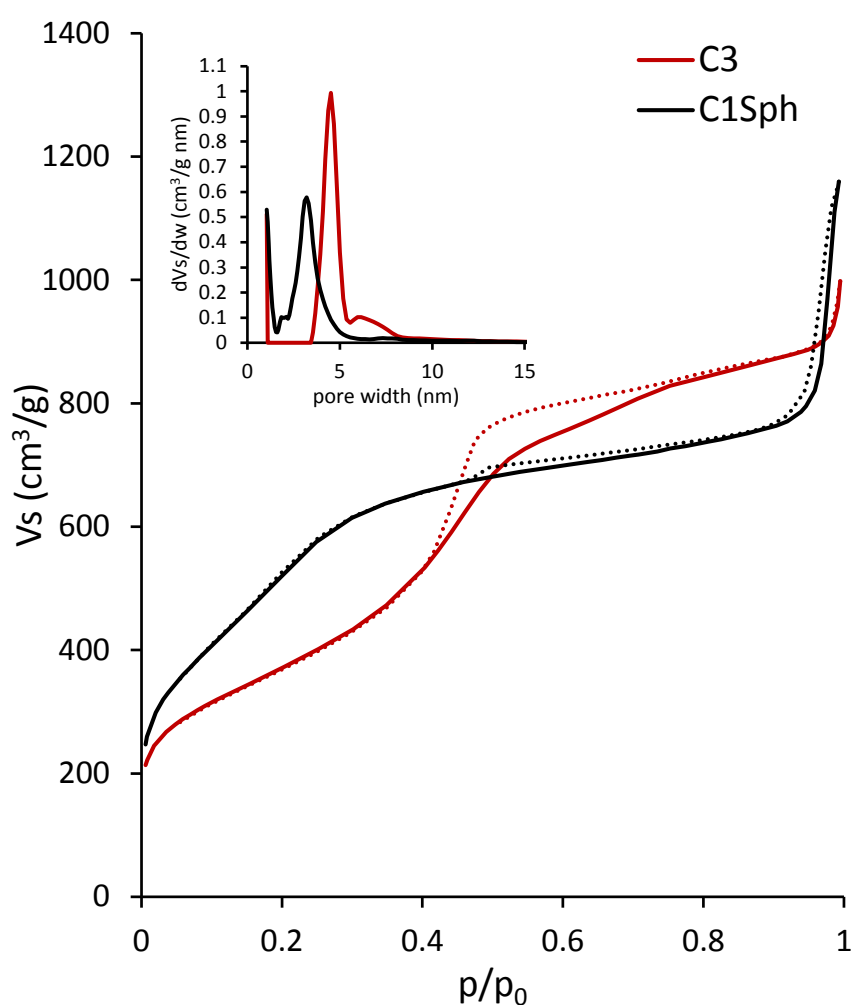

Figure S5: N_2 adsorption isotherms of C3 and C1Sph. Inset: Pore size distribution.

XPS analysis of C3 and C1Sph

The pristine mesoporous carbon materials were also evaluated through X-ray photoelectron spectroscopy (XPS) to investigate their surface chemistry and develop a grafting method (Figure **S6**).
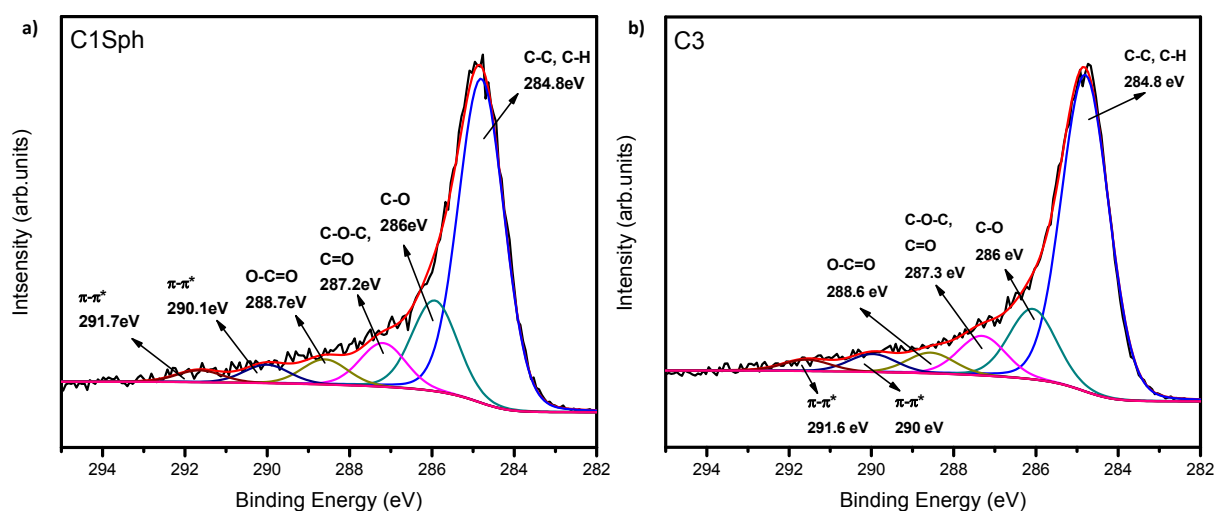

Figure S6. C1s photoelectron spectra of pristine a) C1Sph and b) C3. The expected signals for this type of carriers was obtained, showing presence of hydroxyl, carboxyl and epoxy groups.

Figures **S6**a and **S6**b present the C1s photoelectron spectra of the initial carbon C1Sph and C3 respectively. As shown, the spectrum of C1Sph (Figure

S6a) can be decomposed into six peaks located at 284.8 eV, 286 eV, 287.2 eV, 288.7 eV, 290.1 eV and 291.7 eV. The first peak is attributed to the aliphatic C-C and/or C-H bonds of the main sp^3 carbon frame. The peak at 286 eV represents the hydroxyl C-O bonds on the surface of the plain carbon. Next fitted photoelectron peak at 287.2 eV arises from the contribution of C-O-C epoxy/ether and C=O carbonyl groups which decorate the carbon nanoparticles;[4] the instrumental resolution does not allow the distinction of these groups. The carboxyl groups are displayed at 288.7 eV completing the oxygen functionalities of C1Sph. The next two fitted peaks may be attributed to the π-π* shake up features of the carbon matrix of the material.[4–7] The C3 spectrum is similar to C1Sph. Carbon-carbon bonds are located at 284.8 eV, while C-O bonds at 286.0 eV. Epoxy/ether and carbonyl groups are centered at 287.3 eV and carboxyl groups are located at 288.6 eV similar to the C1Sph. The satellite features at 290 and at 291.6 eV again probably represent the π–π* (HOMO–LUMO) transition of the turbostratic structure of the carbon nanomatrix.[6] It should however be mentioned that signals at 290.0 eV have been also related in the literature to C bonded as CO_3^{2-} (surface carbonates)[7–9] while features around 291.7eV have been assigned to carbon atoms bound to more electronegative fluorine (C-F_2 moieties).[8,10,11]

Grafting protocol

Since the carbon surfaces of both samples have a significant content of oxygen functionalities (C-OH hydroxyl, C-O-C epoxy, -C(=O)-O carboxyl) the most facile approximation of the grafting process seems to be the interaction of the terminal hydroxyl group (C-OH) of the self-immolative polymer with these functional groups through the formation of C-O-C ether groups. One of these possible cases of grafting (i.e., epoxy ring opening) is shown in Scheme S2.
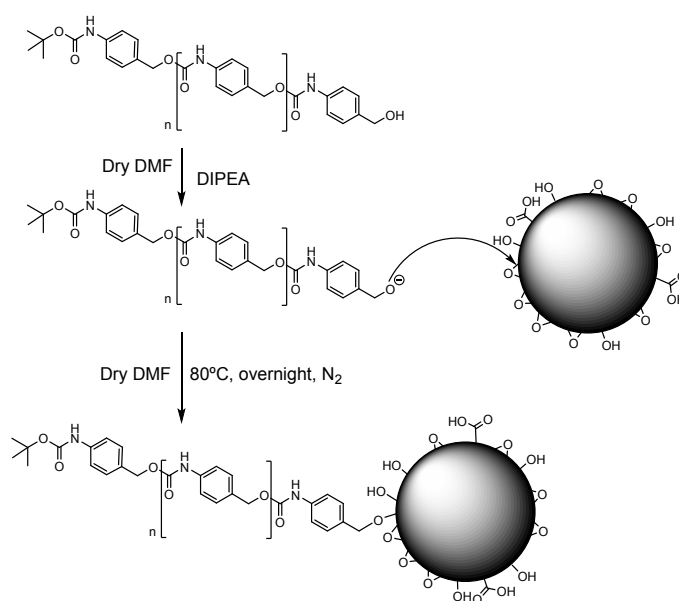
Scheme S2. Grafting strategy of self-immolative polymers on the carbon powders.

TEM microscopy of the coated and unmodified carbon materials

TEM analysis was also carried out to determine if coated carbon particles presented organic matter on their surface. Prior to visualization, both bare and hybrid carbon samples were stained with phosphotungstic acid to visualize the organic matter. In agreement with the previous characterization, a blurrier surface

was observed for the SIP coated particles as illustrated in **Figure S7**b and **S7**d, which can be attributed to the presence of the organic surface layer due to the coating treatment.
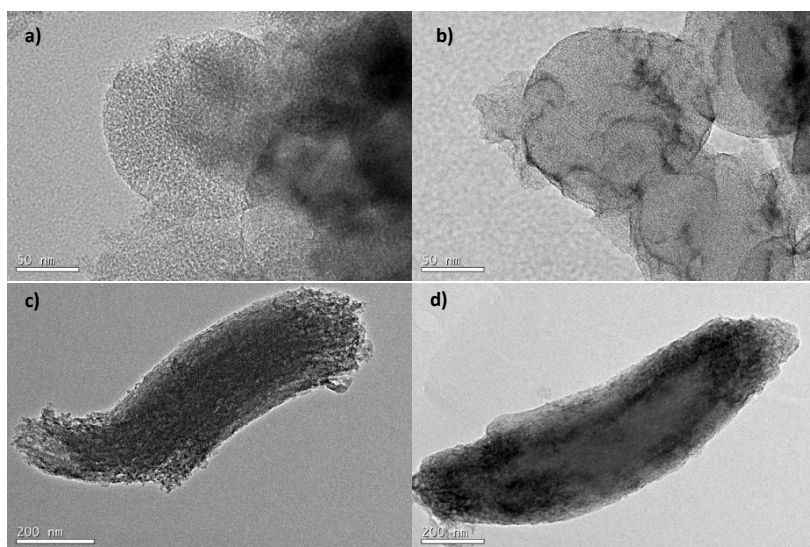

Figure S7. TEM images of a) C1Sph, b) C1Sph-SIP, c) C3 and (d) C3-SIP particles.

Thermogravimetric analysis of SIP-coated *vs.* C3 and C1Sph

The amount of additional organic matter on the samples after the SIP coating was evaluated through thermogravimetric analysis (Figures S8 and S9).
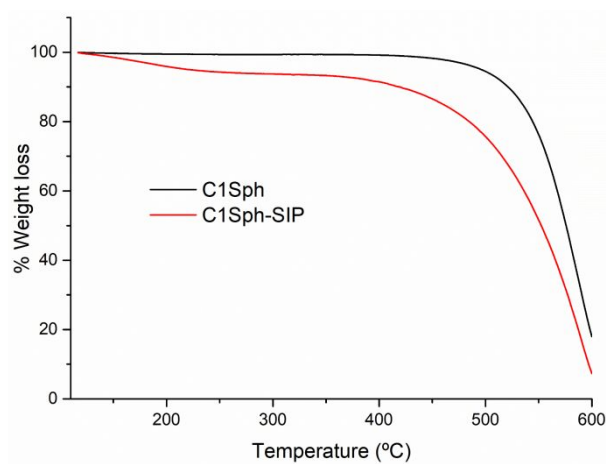
Figure S8. TGA of C1Sph vs C1sph-SIP. The low temperature (<300ºC) weight

loss of C1Sph-SIP indicates the presence of new organic matter on the carrier
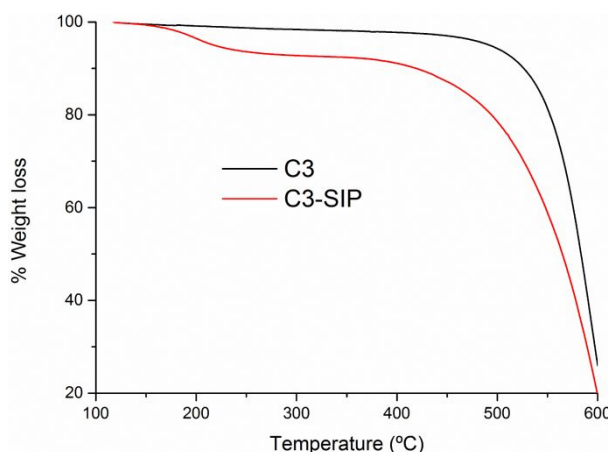
due to the successful coating.

Figure S9. TGA of C3 vs C3-SIP. The low temperature (<300ºC) weight loss of

C3-SIP indicates the presence of new organic matter on the carrier due to the

successful functionalization.

N$_2$ adsorption-desorption measurements of SIP-coated materials *vs.* pristine C3 and C1Sph

The SIP-coated carbons were evaluated using N$_2$ adsorption-desorption

analysis to find out the effect of the polymeric coating on the textural parameters

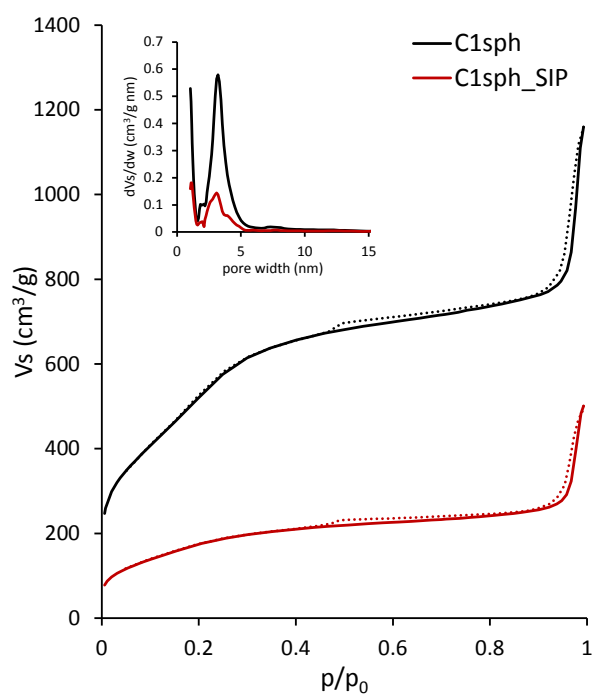of the carbons (Figures S**10** and S**11**).

Figure S10. N_2 sorption-desorption isotherms (77 K) of C1Sph and C1Sph-SIP. The reduction in the amount adsorbed indicates the successful surface deposition of the polymer that blocks a significant part of the pore network.

Figure S11. N_2 sorption-desorption isotherms of C3 and C3-SIP. The reduction in the amount adsorbed indicates the successful surface deposition of the polymer that blocks a significant part of the pore network.
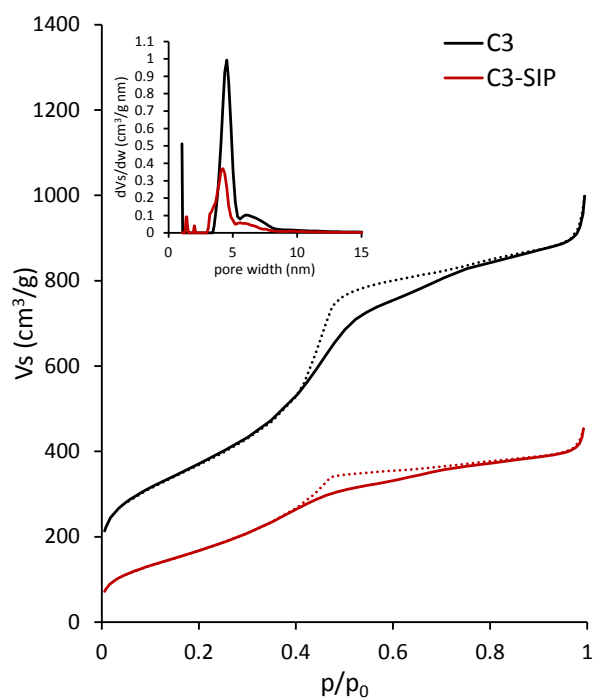
DLS measurements

As mentioned in the manuscript, the modification of the surface of the carbon powders with the self-immolative coating improved their colloidal stability, which was tested by means of DLS measurements on pristine and SIP-coated samples (Figure **S12**).
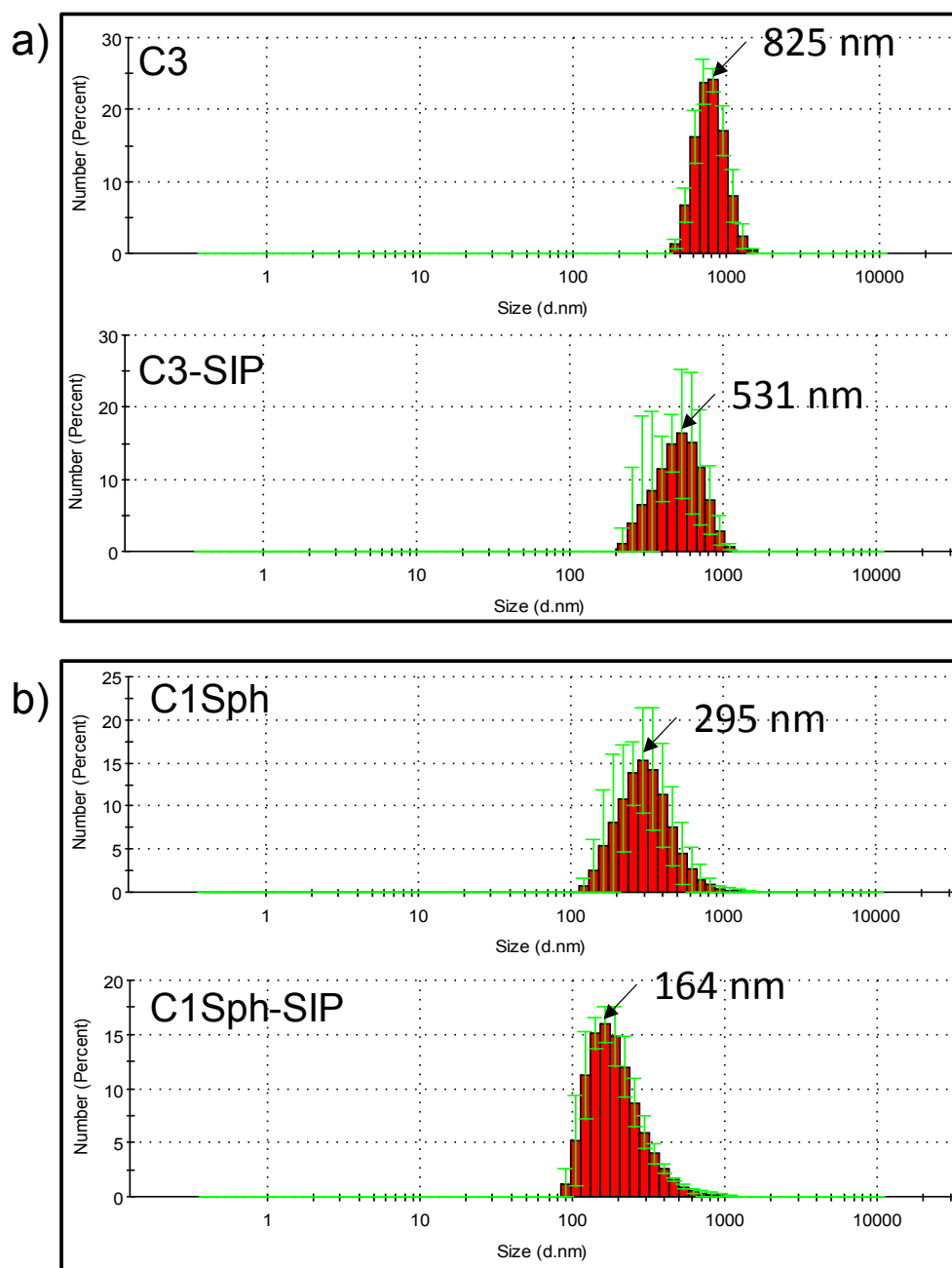
Figure S12. DLS measurements of bare carbons and SIP-coated carbons. The functionalization with the SIP coating enhanced their colloidal stability.

As observed in Figure **S12**, the functionalization with the polymeric coating enhanced the dispersion of the carbon materials (reduced sizes after coating imply limited aggregation, leading to size distributions that are in agreement with the primary particle sizes observed in the SEM microscope. It should be noted

that the diameters measured through DLS experiments are a function of how particles diffuse in a fluid (hydrodynamic diameters) and the calculations are always based on spherical geometry. This situation is directly related to the actual sizes of C1Sph particles, however, for the case of non-spherical particles (such as C3) the results should not be interpreted as real sizes but rather as the diameter of spheres that have the same translational diffusion coefficients with the actual particles.

Thermal stability of SIP-coated carbons

DLS was also employed in order to investigate the thermal stability of the SIP-coated mesoporous carbons. For that purpose, their colloidal stability was investigated before and after heating the hybrid samples in an oven at 75ºC for 4 days (Figure S13). These conditions were chosen to simulate an extreme environment, much harsher than that found in the organism (37ºC).
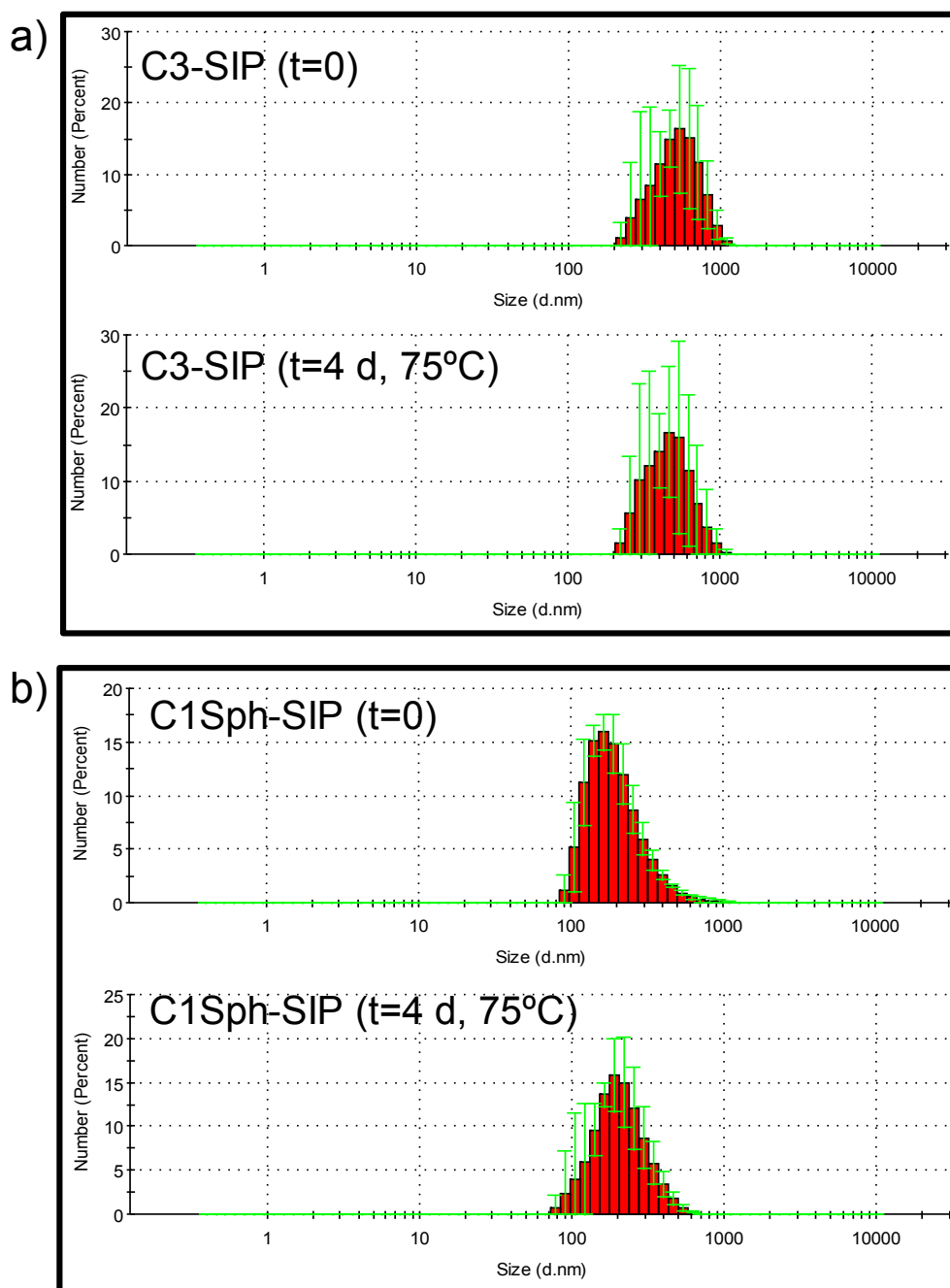
Figure S13. Analysis of the thermal stability of the SIP-coated samples. The samples were subjected to DLS analysis and then they were maintained in an oven at 75ºC for 4 days. After that, the samples were measured again. a) C3-SIP. b) C1Sph-SIP.

As observed in Figure S13, the colloidal dispersibility of both SIP-coated mesoporous carbons remained essentially unaltered after the thermal treatment at 75ºC for 4 days (and certainly much better than the dispersibility of the pristine

nanoparticles, see Figure S**12**). Moreover, this study, in combination with Figure 7A (no significant payload release after 96 hours) confirmed that the SIP-coated mesoporous carbons were stable over the time and that they could be administered in the organism without caring about potential degradation and subsequent premature drug release.

Calculation of the grafting density

The density of polymers grafted to nanoparticles is typically calculated on the basis of their external "geometrical" surface area. In our case we may assume cylindrical (C3) and spherical (C1Sph) particles which have a specific surface area of $2/(r{\cdot}d)$ and $3/(r{\cdot}d)$, respectively (r is the particle radius and d its mass density; for porous particles d is the apparent density that is related with the total volume, i.e. solid and pores). Following the above we have measured the skeletal density of the samples by helium pycnometry (2.1 g/cm^3 for both samples) and calculated the apparent density (0.53 g/cm^3 for C3 and 0.60 g/cm^3 for C1Sph) with the aid of their pore volume (1.4 and 1.2 cm^3/g, respectively). The above lead to "external areas" of *ca.* 28 m^2/g for C3 and 67 m^2/g for C1Sph. Based on the amount of SIP measured by TGA (ca. 15%wt, Figures S**11** and S**12**) we may then derive grafting densities of 6.3 mg/m^2 (1.9 μmol/m^2) for C3 and 2.6 mg/m^2 (0.8 μmol/m^2) for C1Sph. However, it should be stressed that these values are not descriptive for our nanoparticles and are only provided for comparison. This is due to the fact that the external surfaces of the porous carbon particles are not

smooth as assumed above; on the contrary they are very rough (due to their porosity) as clearly evidenced in SEM (and TEM) pictures and simple geometrical models fail completely to describe the surface that is available for grafting. In this respect, a better approximation of the external particle surface is based on sorption measurements and the calculation of the surface that remains available after filling the micro- and meso-pores of the particles. This calculation can be carried out by means of the t- or α_s-plots, which are practically a comparison of the investigated systems with a model isotherm for non-porous solids[2]. Following the above and adopting the de Boer model isotherm, external areas of 103 and 130 m^2/g were deduced for C3 and C1Sph, respectively. These areas certainly lead to lower grafting densities of 1.7 mg/m^2 (0.5 µmol/m^2) for C3 and 1.4 mg/m^2 (0.4 µmol/m^2) for C1Sph, which are very similar for both samples. This is expected since both carbons were produced by carbonization of the same carbon source and thus share the same surface chemistry.

XPS analysis of C3-SIP and C1Sph-SIP

A detailed analysis of the deconvolution of the C1s peaks for the pristine and hybrid materials is shown in table S1.

Table S1. Analysis of the deconvoluted C1s peaks from XPS of C1sph and C3 before and after reaction with SIP.

Peak Assignment	Binding Energy (eV)	C1sph (at. %)	C1sph-SIP (at. %)	C3 (at. %)	C3-SIP (at. %)
C-C / C-H	284.8	63.0	61.7	66.4	59.5
C-O / C-N	286.0	17.6	18.5	14.8	17.9
C-O-C / C=O	287.2 ± 0.1	8.5	8.5	8.3	10.2
O-C=O / N-C=O	288.7 ± 0.1	4.8	5.1	4.3	6.4
CO_3^{2-} / pi-pi* / NH-C(=O)-O	290.1 ± 0.1	3.8	4.0	3.8	4.1
pi-pi* / CF_2	291.7 ± 0.1	2.3	2.2	2.4	1.9

It may be furthermore noteworthy that a small amount of F moieties was detected in the case of C1Sph as indicated from the Survey presented (**Figure S14**). This may be due to surface bonding of fluorine atoms during HF treatment or even inadequate washing of the material following the dissolution of the silica template with HF. In the case of C3, the peak of F was not observed.
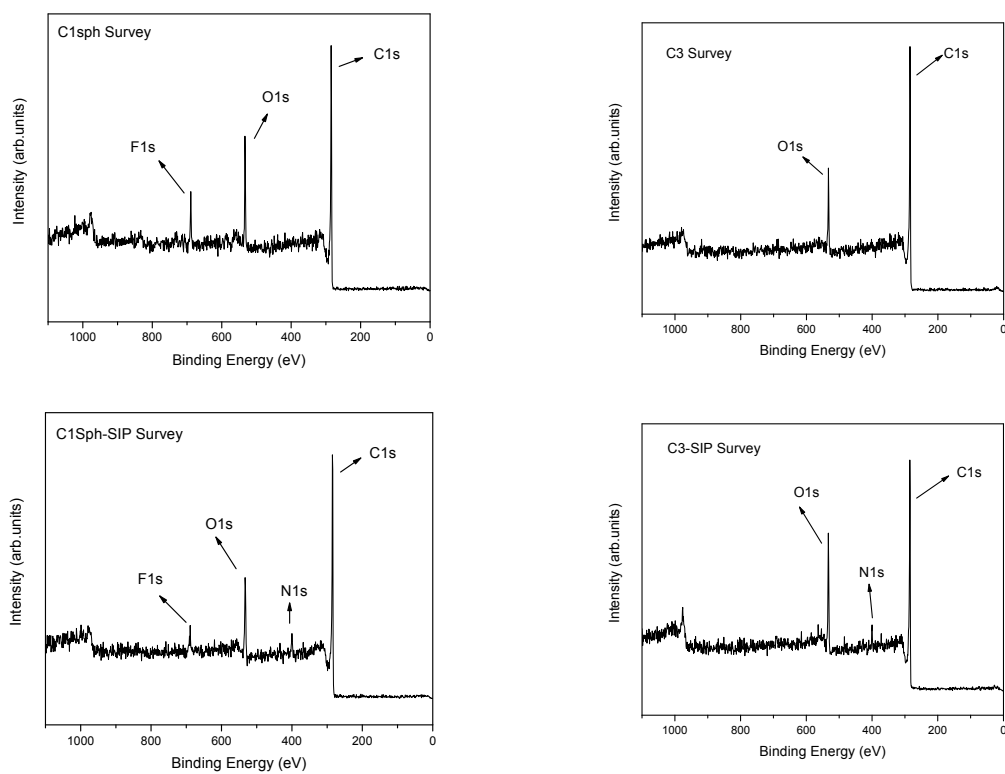
Figure S14. XPS Survey of plain and SIP-coated carbons.

References

(1)   Ryoo, R.; Joo, S. H.; Jun, S. Synthesis of Highly Ordered Carbon Molecular Sieves via Template-Mediated Structural Transformation. *J. Phys. Chem. B* **1999**, *103*, 7743–7746.

(2)   Kruk, M.; Jaroniec, M.; Ryoo, R.; Joo, S. H. Characterization of Ordered Mesoporous Carbons Synthesized Using MCM-48 Silicas as Templates. *J. Phys. Chem. B* **2000**, *104*, 7960–7968.

(3)   Ryoo, B. R.; Joo, S. H.; Kruk, M.; Jaroniec, M. Ordered Mesoporous Carbons. *Adv. Mater.* **2001**, *13*, 677–681.

(4)   Ederer, J.; Janoš, P.; Ecorchard, P.; Tolasz, J.; Štengl, V.; Beneš, H.; Perchacz, M.; Pop-Georgievski, O. Determination of Amino Groups on Functionalized Graphene Oxide for Polyurethane Nanomaterials: XPS Quantitation vs. Functional Speciation. *RSC Adv.* **2017**, *7*, 12464–12473.

(5)   Spyrou, K.; Calvaresi, M.; Diamanti, E. K.; Tsoufi, T.; Gournis, D.; Rudolf, P.; Zerbetto, F. Graphite Oxide and Aromatic Amines : Size Matters. *Adv. Funct. Mater.* **2014**, *25*, 263–269.

(6)   Giasafaki, D.; Charalambopoulou, G.; Tampaxis, C.; Dimos, K.; Gournis, D.; Stubos, A.; Steriotis, T. Comparing Hydrogen Sorption in Different Pd-Doped Pristine and Surface-Modified Nanoporous Carbons. *Carbon* **2016**,

98, 1–14.

(7)   VanDelinder, V.; Wheeler, D. R.; Small, L. J.; Brumbach, M. T.; Spoerke, E. D.; Henderson, I.; Bachand, G. D. Simple, Benign, Aqueous-Based Amination of Polycarbonate Surfaces. *ACS Appl. Mater. Interfaces* **2015**, *7*, 5643–5649.

(8)   Moulder, J. F.; William F. Stickle; Sobol, P. E.; Bomben, K. D. *Handbook of X-Ray Photoelectron Spectroscopy*; Perkin-Emler Corporation, 1992.

(9)   Webb, M. J.; Palmgren, P.; Pal, P.; Karis, O.; Grennberg, H. A Simple Method to Produce Almost Perfect Graphene on Highly Oriented Pyrolytic Graphite. *Carbon* **2011**, *49*, 3242–3249.

(10)   Ferraria, A. M.; Lopes da Silva, J. D.; Botelho do Rego, A. M. XPS Studies of Directly Fluorinated HDPE: Problems and Solutions. *Polymer (Guildf).* **2003**, *44*, 7241–7249.

(11)   Lei, Y. G.; Ng, K. M.; Weng, L. T.; Chan, C. M.; Li, L. XPS C 1s Binding Energies for Fluorocarbon-Hydrocarbon Microblock Copolymers. *Surf. Interface Anal.* **2003**, *35*, 852–855.